A Beamforming-Aided Full-Diversity Scheme for Low-Altitude Air-to-Ground Communication Systems Operating With Limited Feedback

Rakshith Rajashekar, *Senior Member, IEEE*, Marco Di Renzo, *Senior Member, IEEE*, K. V. S. Hari, *Fellow, IEEE*, and Lajos Hanzo, *Fellow, IEEE*

Abstract—Unmanned aerial vehicles (UAVs) have gained a significant popularity in the recent past owing to their easy deployability and wide range of applications. In most of the short- and medium-range applications, Wi-Fi is used as the access technology for establishing communication between the ground stations and the UAVs. Although Wi-Fi is known to perform well in most of the scenarios, it is important to note that Wi-Fi has been mainly designed for indoor communication in rich scattering environments, whereas the air-to-ground (A2G) channel is characterized by sparse scattering. Considering this important difference in the channel characteristics, we revisit some of the Wi-Fi features and propose efficient design alternatives. First, we provide a statistical model for the sparse A2G channel and design an optimal time-domain quantizer (TDQ) for its feedback. In contrast to the frequency-domain quantizer (FDQ) of the IEEE 802.11n/ac Standard, the proposed TDQ exploits the time-domain sparsity in the channel and requires about 15 times lesser quantization bits than FDQ. Second, we propose a beamforming (BF) scheme with the aid of full-diversity rotation (FDR) matrices and analytically evaluate its symbol error probability in order to quantify the attainable diversity order. Our numerical simulations demonstrate that the proposed FDR-BF scheme outperforms the relevant benchmark schemes in both coded as well as uncoded scenarios. Specifically, the proposed FDR-BF scheme was observed to attain a signal-to-noise ratio gain as high as 6dB compared with the popular geometric mean decomposition-based BF scheme, when operating at an elevation angle of $7.5°$.

Index Terms—Low-altitude platforms, drones, beamforming, time-domain quantization, IEEE 802.11.

R. Rajashekar and L. Hanzo are with the School of ECS, University of Southampton, Southampton SO17 1BJ, U.K. (e-mail: rmr1u14@soton.ac.uk; lh@ecs.soton.ac.uk).

M. Di Renzo is with the Laboratoire des Signaux et Systèmes, CNRS, CentraleSupélec, University of Paris-Sud, Université Paris-Saclay, 91192 Gif-sur-Yvette, France. (e-mail: marco.direnzo@l2s.centralesupelec.fr).

K. V. S. Hari is with the Department of ECE, Indian Institute of Science, Bengaluru 560012, India (e-mail: hari@ece.iisc.ernet.in).

Color versions of one or more of the figures in this paper are available online at http://ieeexplore.ieee.org.

I. INTRODUCTION

THE future wireless infrastructure is envisaged to grow beyond the terrestrial realm owing to the rapid proliferation of easily deployable unmanned aerial vehicles (UAV), such as drones, tethered helikites, mini aircrafts etc. [1]–[4]. Among these UAVs, drones have gained significant popularity owing to their wide range of applications such as video surveillance, mapping, safe inspection of power lines/cell towers, search and rescue operations, crop-surveying etc. In the event of a disaster, a robust and reliable network, which can be promptly deployed, becomes necessary for aiding the disaster management operations as well as for providing temporary coverage over the disaster-struck region. Drones deployed as low-altitude platforms (LAPs)[1] [5] that provide connectivity via wireless fidelity (WiFi), or worldwide interoperability for microwave access (WiMAX) and terrestrial trunked radio (TETRA) were experimentally studied in [6], while that relying on long term evolution-advanced (LTE-A) was studied in [7]. Adaptive modulation and coding was designed in [8]. Among these diverse wireless access technologies, WiFi has gained a significant popularity among drones [9]–[14] owing to its ubiquity and versatile *infrastructure* based and *ad-hoc* modes of operation, which are sufficient to cater for a wide range of applications. Specifically, Wu *et al.* [9] studied the robustness of IEEE 802.11a in the presence of high doppler shifts, while Yanmaz *et al.* [10] studied the impact of both the 3D dynamics and of the orientation of the UAVs on the performance of an 802.11a network. In [11], Asadpour *et al.* have evaluated the impact of a) both the distance and of the relative speed between the UAVs; b) the orientation of the antennas and the trajectory of the UAVs; c) the energy efficiency and the data rate, on the performance of an 802.11n network. In [12], Yanmaz *et al.* have studied the performance of the infrastructure and mesh modes of 802.11a, both in single and dual-hop communication scenarios. By contrast, Hayat *et al.* [13] have studied the performance of multi-UAV aided communication in 802.11a and 802.11ac networks. In [14], Guillen-Perez *et al.* have studied the performance of both infrastructure-based and ad-hoc modes of 802.11 in terms of throughput, coverage area and energy efficiency. In [15],

---

[1]LAPs are deployed in the lower troposphere, where as high altitude platforms (HAP) are deployed in the stratosphere.

Jamal and Matolak investigated multiple antenna and diversity techniques in multicarrier communication systems and showed that receive antenna separation increases the diversity gain of the system at short link distances. In [16], Zhang and Hui studied the adaptive MIMO antenna array where the antenna spacing was optimized to reduce the channel correlation and maximize the system capacity. In [17], Chen *et al.* implemented and studied the performance of a long-range broadband aerial communication system using directional antennas.

The classic singular value decomposition (SVD) based beamforming [18] yields parallel sub-channels with unequal signal-to-noise ratios (SNR). The optimal water-filling power allocation [18] would simply assign zero power to some of the low-SNR parallel sub-channels. This would require non-uniform bit-loading, which is practically infeasible. When using uniform bit-loading across all the sub-channels, the effective bit error ratio (BER) performance will be dominated by the sub-channels having low SNRs. Some of the existing solutions that attempt to address this issue include the popular geometric mean decomposition (GMD) based beamforming [19], [20], the uniform channel decomposition (UCD) based beamforming [21], and the space-time block coding (STBC) aided beamforming schemes [22]–[26]. The GMD based beamforming provides identical SNRs across the subchannels, but does not provide any transmit diversity gain, while the UCD based beamforming overcomes this impediment, but at a high computational complexity. The STBC aided beamforming schemes attain the transmit diversity gain at the cost of multiplexing gain.

Although the extensive experimental studies of [9]–[14] confirm that WiFi may indeed be used in LAPs, several of its enhancements/features would be suboptimal in aerial communication scenarios, since its features were designed for indoor wireless channels, which are characterized by rich multipath scattering, whereas the air-to-ground (A2G) wireless channel is characterized by sparse multipath scattering [27]–[30]. Specifically, the delay spread of the indoor channel is not expected to vary significantly, whereas that of the air-to-ground channel may vary significantly, depending on the elevation of the UAV with respect to the ground station [27]. Furthermore, the A2G channel would have a strong line-of-sight (LoS) component, whereas the indoor channel will not have a LoS component in general. Thus, the features of 802.11 that are designed by taking into account the channel characteristics, such as the cyclic prefix (CP), channel quantization, beamforming etc. have to be revisited in the context of A2G communication.

Against this background, the contributions of this paper are as follows:

1) While the various channel measurements found in the literature [27]–[30] provide significant insight into the nature of the A2G channel, they cannot be readily utilized for system design and performance evaluation. A statistical channel model [31], which can be readily tuned for different aerial scenarios would be highly beneficial. In this paper, we first propose a simple statistical channel model and provide the specific model parameters that fit the A2G channel measurement data given in [27] for the elevation angles of $\Psi \in \{7.5°, 15°, 22.5°, 30°\}$. We use this channel model for designing the time-domain channel quantizer as well as for the performance evaluation of the proposed scheme.

2) One of the important features provided by the 802.11n/ac standard [32] is the beamforming[2] [33]–[36], which exploits the knowledge of channel state information (CSI) at the transmitter for improving the transmission range. A key requirement of beamforming is the availability of the CSI at the transmitter, which is accomplished by the frequency domain quantizer (FDQ) employed in 802.11n/ac (20.3.12.3.2 [32]). In contrast to this, motivated by the time-domain sparsity of the A2G channel (Sec. V, Sec. VI, and Sec. III-E in [27], [28], and [29] resp.), we propose a practically motivated time-domain quantizer (TDQ) [35], [37] that operates at the *rate-distortion limit* [38]. Furthermore, we show that the proposed TDQ would significantly reduce the feedback overhead involved in the beamforming, while attaining the same performance as that of FDQ.

3) In contrast to the existing beamforming schemes [19]–[26] discussed earlier, we propose a full-diversity rotation (FDR) [39]–[41] aided beamformer (FDR-BF) that attains the maximum achievable transmit diversity gain without compromising the multiplexing gain. Furthermore, the proposed scheme is shown to attain a significant performance gain over the existing schemes.

The remainder of the paper is organized as follows. The A2G statistical channel model as well as the proposed TDQ are presented in Section II-A and Section II-B, respectively. The proposed FDR based beamforming as well as its diversity analysis are presented in Section III. Our simulation results and discussions are provided in Section IV, while Section V concludes the paper.

Notations: A circularly symmetric complex-valued Gaussian distribution with mean μ and variance σ^2 is represented by $\mathcal{CN}(\mu, \sigma^2)$. An upper truncated Weibull distribution with shape parameter k, scale parameter λ and truncating point B is represented by $\mathcal{WB}(k, \lambda, B)$. The notations of $(\cdot)^H$ and $(\cdot)^T$ indicate the Hermitian transpose and transpose of a vector/matrix, respectively, while $|\cdot|$ represents the magnitude of a complex quantity, or the cardinality of a given set. The uppercase boldface letters represent matrices and lowercase boldface letters represent vectors. The notations of $\|\cdot\|_F$, $\|\cdot\|_0$ and $\|\cdot\|$ represent the Frobenious norm of a matrix, the l_0-norm of a vector and the l_2-norm of a vector, respectively. $\mathbf{H}([c:d],:)$ represents a matrix with rows $c, c+1, \ldots, d-1, d$ of $\mathbf{H}$ and $\mathbf{H}(:,[c:d])$ is a matrix with columns $c, c+1, \ldots, d-1, d$ of $\mathbf{H}$. The kth element of a vector $\mathbf{s}$ is denoted by $\mathbf{s}(k)$. Expected value of a random variable Y is denoted by $\mathbb{E}(Y)$. Furthermore, $Q(x)$ represents the tail probability of standard normal

---

[2]Note that the 802.11 standard provides both implicit and explicit beamforming features (20.3.12.2 and 20.3.12.3 in [32]) resp.). Throughout this paper, we consider only the explicit beamforming with CSI matrices feedback as detailed in 20.3.12.3.2 in [32].

distribution given by $\frac{1}{\sqrt{2\pi}}\int_x^\infty \exp\left(-\frac{u^2}{2}\right)du$. $\mathbb{C}$ and $\mathbb{R}$ represent the field of complex and real numbers, respectively.

II. STATISTICAL A2G CHANNEL MODEL AND THE PROPOSED TIME-DOMAIN QUANTIZER

In this section, we first present our statistical model of the A2G channel, which is based on the measurement data of [27], followed by our proposed TDQ for the A2G channel, which imposes very low feedback overhead compared to the conventional FDQ [32].

A. Statistical A2G Channel Model

Let L_t denote the number of multipath components between the ground station and the aerial transmitter deployed as a LAP. Let α_i and τ_i denote the complex-valued gain and the delay associated with the ith multipath component, respectively. The multipath channel is given by

$$h(\tau) = \sum_{i=0}^{L_t-1} \alpha_i \delta(\tau - \tau_i), \qquad (1)$$

where we have $\alpha_i \sim \mathcal{CN}(0, \sigma_i^2)$, $\sigma_i = \Omega\beta^i$, $1 \leq i \leq L_t - 1$, $0 < \beta \leq 1$, $h(\tau)$ is the impulse response of the channel, $\delta(x) = 1$ if $x = 0$ and 0 otherwise. The normalization factor Ω is chosen so that $\Omega\sum_{i=0}^{L_t-1}\beta^i = 1$. Furthermore, α_0 is modeled as a Rician fading component with the ratio of power in the LoS component compared to that of non-LoS component denoted by K, i.e. $\alpha_0 \sim \sqrt{\frac{K}{1+K}}\sigma_0 + \sqrt{\frac{1}{1+K}}\mathcal{CN}(0, \sigma_0^2)$. The multipath delays are modeled by statistically independent truncated Weibull random variables, i.e. $\tau_i \sim \mathcal{WB}(k, \lambda, B)$ $\forall i$.

It was observed in [27] (Section V) that the average number of paths in the LAP scenario is 7.88. Thus, we consider $L_t = 8$ for all the four elevation profiles in our model. Furthermore, considering a power margin of 25dB with respect to the strongest multipath component, the limits of the excess delay for elevation angles of $7.5°, 15°, 22.5°, 30°$ are given by 1550ns, 1480ns, 1294ns, 1290ns (Table 2, [27]), respectively. Thus, we consider $B \in \{1550, 1480, 1294, 1290\}$ for the four elevation profiles. Furthermore, the choice of $\lambda \in \{1000, 460, 205, 161\}$, $K(dB) \in \{0, 6, 12, 20\}$, $\beta \in \{0.27, 0.26, 0.26, 0.24\}$ and $k = 1.1$ for all the elevation profiles results in an average root mean squared (RMS) delay spread [18] similar to that of the measured data (refer to [27, Table 1]). The RMS delay spread for a given channel realization is given by $\frac{\sum_i |\alpha_i|^2(\tau_i-\hat{\tau})^2}{\sum_i |\alpha_i|^2}$, where $\hat{\tau} = \frac{\sum_i \tau_i|\alpha_i|^2}{\sum_i |\alpha_i|^2}$, $0 \leq i \leq L_t - 1$ in all the summations. The parameters of the A2G channel model for various elevation angles are provided in Table I. The mean RMS delay spread recorded for the various elevation angles based on the measured data as well as that obtained by the channel model considered above are listed in Table II. It is evident from Table II that the mean RMS delay spread computed using the statistical channel model is quite close that of the measured data [27]. Furthermore, the complementary cumulative distribution function (CCDF) function of the RMS delay spread recorded for various elevation angles and computed based on the proposed statistical channel model

TABLE I
MODEL PARAMETERS FOR THE PROPOSED STATISTICAL A2G CHANNEL MODEL

Elevation angle (Ψ)	K-factor of the LoS path (dB)	Multipath delay parameters (k, λ, B)	Multipath variance parameter (β)
7.5^o	0	$(1.1, 1000, 1550)$	0.27
15°	6	$(1.1, 460, 1480)$	0.26
22.5^o	12	$(1.1, 205, 1294)$	0.26
30°	20	$(1.1, 161, 1290)$	0.24

TABLE II
COMPARISON OF THE MEAN RMS DELAY SPREAD - MEASURED DATA [27] VS. STATISTICAL CHANNEL MODEL

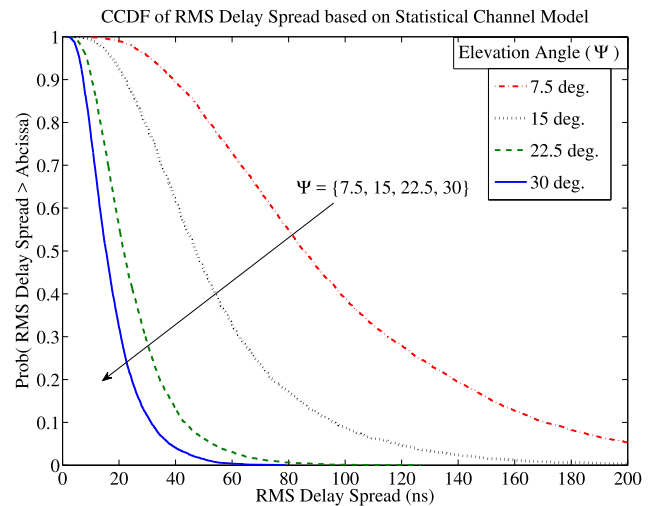| Elevation angle (Ψ)	Mean RMS Delay Spread (ns) from **Measured Data [27]**	Mean RMS Delay Spread (ns) from **Statistical Model**
7.5^o	98.1	95.8
15°	54.9	54.7
22.5^o	24.3	24.8
30°	18.3	17.8

Fig. 1. The CCDF of RMS delay spread for elevation angles $\Psi \in \{7.5°, 15°, 22.5°, 30°\}$ computed based on the proposed statistical channel model.

is provided in Fig. 1. The CCDF of the RMS delay spread presented in Fig. 1 coincides with that of the measured data presented in [27, Fig. 3]. Thus, we conclude from Table II and Fig. 1 that the proposed statistical channel model is a good approximation of the A2G multipath channel and hence can be utilized for system design and performance analysis.[3]

B. Proposed TDQ for A2G Channel

In MIMO-OFDM systems employing beamforming, CSI is required at the transmitter, which is attained by quantizing the channel at the receiver and sending the same to the transmitter.

[3]Note that we have not considered the channel variation in time due to vehicle dynamics, since we are only interested in the case where the transmission frames do not exceed the channel coherence time.

TABLE III
Optimal Number of Quantization Bits for Various Distortion Levels D_t at the Elevation Angle $\Psi = 7.5°$

Quant. bits	$D_t = 10^{-1}$	$D_t = 10^{-2}$	$D_t = 10^{-3}$	$D_t = 10^{-4}$
B_0	6	10	13	16
B_1	4	8	11	14
B_2	3	6	9	13
B_3	1	4	7	11
B_4	*	2	5	9
B_5	*	*	4	7
B_6	*	*	2	5
B_7	*	*	*	3
Total	14	30	51	78

The 802.11n/ac (20.3.12.3.4 [32]) quantizes the channel in the frequency domain since the indoor channel exhibits rich scattering. However, in A2G link, the channel is sparse and hence offers very low-feedback overhead when quantized in the time domain. In the following we describe the TDQ and its implementation.

Since the K-factor associated with α_0 may vary significantly depending on the elevation angle [27], we consider α_0 to be Gaussian distributed in order to cater for the worst-case scenario. In other words, the Gaussian assumption ensures that α_0 will have maximum number of quantization levels in order to meet the rate distortion limit. Let the multipath channel coefficients be denoted by $\boldsymbol{\alpha} = [\alpha_0, \alpha_1, \ldots, \alpha_{L_t-1}]^T$ and the quantized channel coefficients be denoted by $\boldsymbol{\alpha}^q = [\alpha_0^q, \alpha_1^q, \ldots, \alpha_{L_t-1}^q]^T$. If the total affordable mean-squared distortion is $D_t = \mathbb{E}[\|\boldsymbol{\alpha} - \boldsymbol{\alpha}^q\|^2]$, upon assuming uniform distortion across all the quantized taps, for the average distortion per quantized tap we have D_t/L_t. From [38, Th. 13.3.2], the optimal number of quantization bits for the ith multipath tap is given by

$$B_i = \left[\log_2\left(\frac{\sigma_i^2 L_t}{D_t}\right)\right]_+, \quad (2)$$

where $[x]_+ = \max(x, 0)$. Since it is widely recognized that a uniform scalar quantizer approaches the rate-distortion limit of a Gaussian source up to a constant gap [37], we exploit this for quantizing the real and imaginary parts of the multipath channel coefficients. Let $\bar{B}_i = \lceil \frac{B_i}{2} \rceil$ represent the number of bits available for quantizing the real and imaginary components of the ith multipath coefficient. The quantization interval size is chosen to be [37]:

$$\Delta_i = \sqrt{\frac{4 B_i \sigma_i^2}{\log_2 e}} 2^{-\bar{B}_i}, \quad (3)$$

where $e = 2.7183$. (3) ensures that the distortion (D_t/L_t) decays exponentially with $\bar{B}_i$ for each of the taps. The optimal number of quantization bits for different distortion levels in case of $\Psi = 7.5°$ is provided in Table III. From Table III we see that as D_t reduces from 10^{-1} to 10^{-4}, the number of taps with non-zero bit allocations increases from 4 to 8. Similar observations hold for the other elevation angles as well.

Although the number of analog multipath components is fixed to $L_t = 8$, the number of paths in the digital baseband domain would vary due to the finite sampling resolution. For instance, if $1/W$ is the sampling period, where W is the signal bandwidth, then the paths that fall within the time interval $-1/2W$ to $1/2W$ from the sampling epoch cannot be resolved. Thus, the number L_a of sampled multipath components may not be known to the receiver *a priori*. Assuming a nominal sampling frequency of 20MHz, the digital baseband channel[4] is modeled as

$$h(l) = \sum_{i=0}^{L_a-1} \alpha_{p_i} \delta(l - m_i), \quad (4)$$

where $L_a \le L_t$ and $0 \le m_i \le 31$, which corresponds to a delay of 0ns to 1600ns that caters for a wide range of delays associated with various elevation angles. Among the multipath taps that fall in the interval $j/W \le \tau < (j+1)/W$ ($0 \le j \le 31$), the one closest to the sampling epoch[5] (j/W) is considered to be the sampled tap.

Let $\bar{\boldsymbol{\alpha}} = [\alpha_{p_0}, \alpha_{p_1}, \ldots, \alpha_{p_{L_a-1}}]^T$ represent the set of L_a sampled taps, where $0 \le p_0 < p_1 \cdots < p_{L_a-1} \le L_t - 1$. Note that the receiver may not know the statistics associated with the sampled taps, since the tap-indices p_i are not known *a priori*. Hence, the receiver may not be able to choose the right quantization resolution for each of the sampled taps. This issue is overcome by employing a simple algorithm based on combinatorial search, whose details are given below.

Given that the affordable distortion limit is D_t, the associated maximum number of quantization taps with non-zero quantization bits is given by $L_q = \max\{i \mid 0 \le i \le L_t - 1, B_i > 0\} + 1$, and the associated quantizers be represented by $\mathcal{Q}_0, \mathcal{Q}_1, \cdots, \mathcal{Q}_{L_q-1}$, which employ $B_0, B_1, \ldots, B_{L_q-1}$ quantization bits, respectively. Given $I = \{i_0, i_1, \ldots, i_{|I|-1}\} \subseteq \{i\}_{i=0}^{L_q-1}$, we use the notation $\mathcal{Q}_I$ for representing $[\mathcal{Q}_{i_0}, \mathcal{Q}_{i_1}, \ldots, \mathcal{Q}_{i_{|I|-1}}]^T$. For any given $\mathbf{a} \in \mathbb{C}^{|I|}$, we have $\mathcal{Q}_I : \mathbf{a} \to \mathbf{a}^q$, where $\mathbf{a}^q(k) = \mathcal{Q}_{i_k}[\mathbf{a}(k)]$ for $0 \le k \le |I| - 1$.

Depending on the value of L_a, which in turn depends on the channel realization, two scenarios may arise: $L_q \le L_a$ and $L_q > L_a$. When $L_q \le L_a$, the first L_q out of the L_a taps are quantized. When $L_q > L_a$, we have to search for the appropriate quantization taps that minimize the effective distortion. Let the enumerations of $n = \binom{L_q}{L_a}$ possible combinations be represented by $\{I_i\}_{i=1}^n$, where the elements in each of I_i are assumed to be in ascending order. Let $\mathcal{Q}_{I_j}$ represent the quantizer that considers the quantization taps to be those given by the set I_j. The effective distortion associated with the choice of I_j is $d_j = \|\bar{\boldsymbol{\alpha}} - \mathcal{Q}_{I_j}(\bar{\boldsymbol{\alpha}})\|^2$. The optimal set of quantization taps is the one that provides the least distortion, i.e. $I^* = I_{j^*}$, where $j^* = \arg\min_i d_i$. Algorithm 1 outlines the above combinatorial search.

Fig. 2 compares the average empirical distortion for various elevation angles as a function of the number quantization bits.

---

[4]Considering a sampling frequency of 20MHz and the time-domain sparsity of the A2G channel, the digital baseband channel given in (4) is a fair approximation. When the sampling frequency is high, the effect of transmit and receive front-end filters become prominent and hence should be taken into account.

[5]Sampling epoch is the time instant at which the analog signal is digitized by the analog-to-digital converter (ADC) at the receiver.
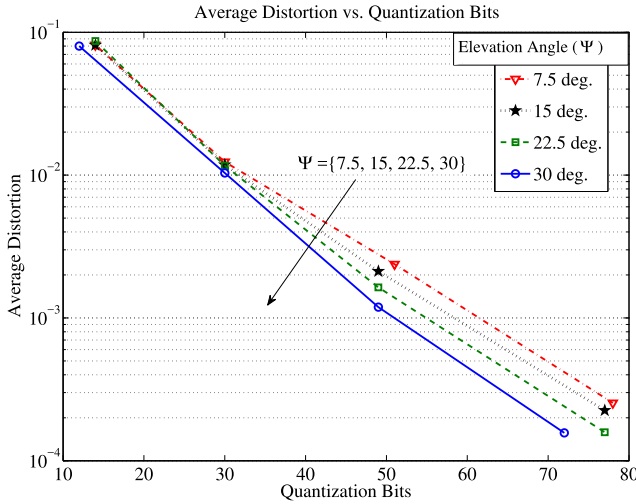

Algorithm 1 Combinatorial Search for Optimal TDQ Taps

Require: $\bar{\alpha}$, L_a, L_q, $n = \binom{L_q}{L_a}$, and $\{I_i\}_{i=1}^n$.

  if $L_q \leq L_a$ **then**

    $I^* = [0, 1, \ldots, L_q - 1]$.

  else

    for $i = 1 : n$ **do**

      $d_i = \|\bar{\alpha} - \mathcal{Q}_{I_i}(\bar{\alpha})\|^2$.

    end for

    $j^* = \arg\min_i d_i$,

    $I^* = I_{j^*}$.

  end if

Fig. 2. Empirical average distortion as a function of quantization bits for various elevation angles. The average distortion is computed by considering thousand independent channel realizations for each of the elevation angles.

It is evident from Fig. 2 that for $\Psi = 7.5°$ the average distortion varies approximately from 10^{-1} to 10^{-4}, as the number of quantization bits is increased from 14 to 78 (refer to Table III), which validates the optimality of the number of quantization bits given in (2) as well as the efficiency of Algorithm 1. Similar observations hold for other elevation angles as well.

Proposed TDQ vs. FDQ of 802.11 [32]: We will show in Section IV that a distortion level of 10^{-2} would be sufficient to attain nearly the same BER performance as that attained with the aid of perfect CSI, and hence 30 bits would be sufficient[6] to quantize each of the links between the transmit and receive antenna pair. That is, a total of $N_{TDQ} = 30N_tN_r$ bits are required in case of the proposed TDQ, where N_t and N_r are the number of transmit and receive antennas, respectively. By contrast, the FDQ of 802.11n/ac would require $N_{FDQ} = (3 + 2\ N_cN_rN_b)N$ bits (20.3.12.3.4 [32]), where N is the number of subcarriers, $N_b \in \{4, 5, 6, 8\}$ is the number of quantization bits and N_c is the number of transmit streams. Note that N_{FDQ} scales with N, whereas N_{TDQ} does not. For instance, with a bandwidth of $W = 20$MHz, we have $N = 52$ data subcarriers. With $N_t = N_r = 2 = N_c$ and

---

[6]Note that the knowledge of delays (m_i) will be available at the transmitter due to channel reciprocity and hence need not be explicitly conveyed.

$N_b = 4$, we have $N_{FDQ} = 1820$ bits. Finally, for the same system configuration, we have $N_{TDQ} = 120$ bits, which is about fifteen times lower than N_{FDQ}.

III. PROPOSED FULL DIVERSITY ROTATION AIDED BEAMFORMING SCHEME

In this section, we first present the system model of the MIMO-OFDM in the time and frequency domains, followed by the proposed FDR-BF scheme which attains the full diversity gain without compromising on the spatial multiplexing gain.

A. System Model

Consider a multiple-input multiple-output (MIMO) aerial communication system having N_t transmit and N_r receive antennas, where the transmitter is carried by a LAP, while the receiver is assumed to be at a fixed location on ground. Let N represent the number of data subcarriers, $N_{SS} = \min(N_t, N_r)$ represent the number of spatial streams and N_{CP} represent the length of CP in terms of the number of samples. Let $\mathbf{F}_N \in \mathbb{C}^{N \times N}$ and $\mathbf{F}_N^\dagger = \mathbf{F}_N^H/N \in \mathbb{C}^{N \times N}$ represent the discrete Fourier transform (DFT) and inverse DFT matrices [18], respectively, i.e. $\{\mathbf{F}_N\}_{m,n} = e^{-j2\pi(m-1)(n-1)/N}$ for $1 \leq m, n \leq N$. The channel between each of the transmit and receive antenna pairs is modeled as a sparse multipath channel given by (4). Specifically, the channel between the ith receive and the jth transmit antenna is denoted by $\mathbf{h}_{ij} \in \mathbb{C}^{N_{CP}}$ and its frequency-domain representation is given by $\mathbf{h}'_{ij} = \mathbf{F}_N[\mathbf{h}_{ij}^T, \mathbf{0}^T]^T \in \mathbb{C}^N$. Considering orthogonal frequency division multiplexing (OFDM) based transmission [18] with perfect time and frequency synchronization, the received baseband signal at the ith receive antenna after the removal of CP is given by

$$\mathbf{y}_i = \sum_{j=1}^{N_t} \mathbf{H}_{ij}\mathbf{x}_j + \mathbf{n}_i \quad \forall\ 1 \leq i \leq N_r, \tag{5}$$

where $\mathbf{H}_{ij} \in \mathbb{C}^{N \times N}$ represents the circulant matrix corresponding to the channel between the ith receive and the jth transmit antenna. Furthermore, $\mathbf{x}_j \in \mathbb{C}^N$ represents the OFDM symbol in the time-domain transmitted from the jth transmit antenna, while the elements of $\mathbf{n}_i \in \mathbb{C}^N$ are from $\mathcal{CN}(0, \sigma_n^2)$, where σ_n^2 is the noise variance. The signal received at the ith antenna in the frequency-domain is given by

$$\mathbf{y}'_i = \mathbf{F}_N\mathbf{y}_i = \sum_{j=1}^{N_t} \mathbf{F}_N\mathbf{H}_{ij}\mathbf{F}_N^\dagger\mathbf{x}'_j + \mathbf{F}_N\mathbf{n}_i, \tag{6}$$

$$= \sum_{j=1}^{N_t} \mathbf{\Lambda}_{ij}\mathbf{x}'_j + \mathbf{n}'_i, \tag{7}$$

where $\mathbf{\Lambda}_{ij} \in \mathbb{C}^{N \times N}$ is the diagonal matrix with $\mathbf{\Lambda}_{ij}(k, k) = \mathbf{h}'_{ij}(k)$ for $1 \leq k \leq N$, while $\mathbf{x}'_j \in \mathbb{C}^N$ represents the frequency-domain symbols transmitted from the jth transmit antenna. The signal received at the kth subcarrier is given by

$$\bar{\mathbf{y}}_k = \bar{\mathbf{H}}_k\bar{\mathbf{x}}_k + \bar{\mathbf{n}}_k \quad \forall\ 1 \leq k \leq N, \tag{8}$$

where we have $\bar{\mathbf{H}}_k(i, j) = \mathbf{\Lambda}_{ij}(k, k)$, $\bar{\mathbf{y}}_k(i) = \mathbf{y}'_i(k)$, $\bar{\mathbf{x}}_k(j) = \mathbf{x}'_j(k)$ and $\bar{\mathbf{n}}_k(i) = \mathbf{n}'_i(k)$ for $1 \leq i \leq N_r$ and $1 \leq j \leq N_t$.

B. Proposed FDR-BF Scheme

Let $\mathbf{P}_k \in \mathbb{C}^{N_t \times N_{SS}}$ represent the beamforming/precoding matrix chosen for the kth subcarrier. The proposed beamformer is given by

$$\mathbf{P}_k = \mathbf{V}_k(:, [1 : N_{SS}]) \boldsymbol{\Phi}_k^{1/2} \boldsymbol{\Theta}_{N_{SS}}, \qquad (9)$$

where $\mathbf{V}_k \in \mathbb{C}^{N_t \times N_t}$ is the right singular matrix of $\bar{\mathbf{H}}_k = \mathbf{U}_k \boldsymbol{\Sigma}_k \mathbf{V}_k^H$, $\boldsymbol{\Phi}_k$ is a diagonal matrix that decides the power allocated over parallel channels at the kth subcarrier based on water-filling [18] and $\boldsymbol{\Theta}_{N_{SS}} \in \mathbb{C}^{N_{SS} \times N_{SS}}$ is the FDR matrix [39]–[41]. Specifically, for the $N_{SS} = 2$ case we have $\boldsymbol{\Theta}_{N_{SS}} = \begin{bmatrix} -0.5257 & -0.8506 \\ -0.8506 & 0.5257 \end{bmatrix}$ [41]. The FDR matrices were originally employed in diagonal STBCs in order to attain full transmit diversity gain [39], [40]. The FDR matrices associated with maximized minimum product distance were designed for $N_{SS} > 1$ and are available in [41]. Note that Bergman and Bjorn [42] and Sakzad and Viterbo [43] also considered a similar precoding scheme as that given by (9), albeit in a different context. Specifically, Svante *et al.* focused on optimizing the bit-loading and $\boldsymbol{\Theta}_{N_{SS}}$ in [42], where no explicit diversity analysis was provided. By contrast, Sakzad and Viterbo [43] studied the unitary precoding scheme conceived for STBCs in the context of an integer-forcing receiver. In contrast to this, we consider the maximum likelihood (ML) receiver, which only requires $\boldsymbol{\Theta}_{N_{SS}}$ to have non-zero minimum product distance in order to attain full transmit diversity. Our proposed scheme ensures water-filling based optimal power allocation in contrast to the existing schemes [42], [43], which employ equal-power allocation. Furthermore, in contrast to the STBC based scheme of [43], our transmission scheme does not require coding over time. Lastly, our method of diversity analysis is different from that of the existing literature.

1) Diversity Analysis: The precoded symbols of the kth subcarrier are given by

$$\bar{\mathbf{x}}_k = \mathbf{P}_k \mathbf{s}_k, \qquad (10)$$
$$= \mathbf{V}_k(:, [1 : N_{SS}]) \boldsymbol{\Phi}_k^{1/2} \boldsymbol{\Theta}_{N_{SS}} \mathbf{s}_k, \qquad (11)$$

where $\mathbf{s}_k \in \mathbb{C}^{N_{SS}}$, whose elements are drawn from a lattice constellation such as the M-QAM signal set. Let $\mathcal{S}$ represent the set of all possible candidate transmit vectors, whose elements are from an M-QAM signal set. Furthermore, let $\Delta\bar{\mathcal{S}} = \{\boldsymbol{\Theta}_{N_{SS}}(\mathbf{s} - \mathbf{s}') \mid \mathbf{s}, \mathbf{s}' \in \mathcal{S}, \mathbf{s} \neq \mathbf{s}'\}$. Owing to the non-zero minimum product distance of $\boldsymbol{\Theta}_{N_{SS}}$ [39], we have $\prod_{i=1}^{N_{SS}} |\bar{\mathbf{s}}(i)| > 0, \forall \ \bar{\mathbf{s}} \in \Delta\bar{\mathcal{S}}$. Let $\delta_{min}^2 = \min_{\bar{\mathbf{s}} \in \Delta\bar{\mathcal{S}}} \min_{1 \leq i \leq N_{SS}} |\mathbf{e}_i^T \bar{\mathbf{s}}|^2$, where $\mathbf{e}_i \in \mathbb{R}^{N_{SS}}$ so that $\mathbf{e}_i(j) = \delta(i - j)$. Given a channel realization $\bar{\mathbf{H}}_k$, the pairwise symbol error probability between $\mathbf{s}, \mathbf{s}' \in \mathcal{S}$ is given by

$$\text{PEP}(\mathbf{s} \to \mathbf{s}' | \bar{\mathbf{H}}_k) = Q\left(\frac{\sqrt{\rho}}{2} \|\bar{\mathbf{H}}_k \mathbf{P}_k(\mathbf{s} - \mathbf{s}')\|\right), \qquad (12)$$
$$\leq \frac{1}{2} \exp\left(-\frac{\rho}{4} \|\bar{\mathbf{H}}_k \mathbf{P}_k(\mathbf{s} - \mathbf{s}')\|^2\right), \qquad (13)$$

where ρ denotes the SNR at each receive antenna and the inequality in (13) follows from the Chernoff bound [44].

Substituting $\mathbf{U}_k \boldsymbol{\Sigma}_k \mathbf{V}_k^H$ for $\bar{\mathbf{H}}_k$ in (13), we have

$$\text{PEP}(\mathbf{s} \to \mathbf{s}' | \bar{\mathbf{H}}_k) \leq \frac{1}{2} \exp\left(-\frac{\rho}{4} \|\boldsymbol{\Sigma}_k \mathbf{V}_k^H \mathbf{P}_k(\mathbf{s} - \mathbf{s}')\|^2\right). \quad (14)$$

Substituting for $\mathbf{P}_k$ from (9), we have

$$\text{PEP}(\mathbf{s} \to \mathbf{s}' | \bar{\mathbf{H}}_k) \leq \frac{1}{2} \exp\left(-\frac{\rho}{4} \|\boldsymbol{\Sigma}_k' \boldsymbol{\Theta}_{N_{SS}}(\mathbf{s} - \mathbf{s}')\|^2\right), \quad (15)$$
$$= \frac{1}{2} \exp\left(-\frac{\rho}{4} \|\boldsymbol{\Sigma}_k' \bar{\mathbf{s}}\|^2\right), \qquad (16)$$

where $\boldsymbol{\Sigma}_k' = \boldsymbol{\Sigma}_k(:, [1 : N_{SS}]) \boldsymbol{\Phi}_k^{1/2}$ and $\bar{\mathbf{s}} \in \Delta\bar{\mathcal{S}}$. If the singular values of $\bar{\mathbf{H}}_k$ are represented by $\bar{\sigma}_k(i)$, $1 \leq i \leq N_{SS}$ and the power allocated for the ith parallel channel is $P_k(i)$ so that $P_{tot} = \sum_{i=1}^{N_{SS}} P_k(i) \ \forall k$, we have

$$\text{PEP}(\mathbf{s} \to \mathbf{s}' | \bar{\mathbf{H}}_k) \leq \frac{1}{2} \exp\left(-\frac{\rho}{4} \sum_{i=1}^{N_{SS}} P_k(i) \bar{\sigma}_k(i)^2 |\bar{\mathbf{s}}(i)|^2\right). \qquad (17)$$

Due to water-filling power allocation [18], we have $P_k(i) = \left(\mu - \frac{1}{\rho \bar{\sigma}_k(i)^2}\right)_+$, where μ satisfies $\sum_{i=1}^{N_{SS}} \left(\mu - \frac{1}{\rho \bar{\sigma}_k(i)^2}\right)_+ = P_{tot}$. Specifically, the *water level* is set to μ and a power allocation of $\mu - \frac{1}{\rho \bar{\sigma}_k(i)^2}$ is allocated to the ith channel if $\mu - \frac{1}{\rho \bar{\sigma}_k(i)^2} > 0$, else no power is allocated to that channel. For further details on water-filling power allocation, please refer to [18, Sec. 5.3.3]. At high SNR, we have $\frac{1}{\rho} \to 0$ and hence $P_k(i) \approx \mu \approx P_{tot}/N_{SS}$. Furthermore, we have $\delta_{min}^2 \sum_{i=1}^{N_{SS}} \bar{\sigma}_k(i)^2 \leq \sum_{i=1}^{N_{SS}} \bar{\sigma}_k(i)^2 |\bar{\mathbf{s}}(i)|^2$ for any channel realization. Thus, we have

$$\text{PEP}(\mathbf{s} \to \mathbf{s}' \mid \bar{\mathbf{H}}_k) \leq \frac{1}{2} \exp\left(-\frac{\rho P_{tot} \delta_{min}^2}{4 N_{SS}} \sum_{i=1}^{N_{SS}} \bar{\sigma}_k(i)^2\right), \qquad (18)$$
$$= \frac{1}{2} \exp\left(-\frac{\rho P_{tot} \delta_{min}^2}{4 N_{SS}} \|\bar{\mathbf{H}}_k\|_F^2\right), \quad (19)$$
$$= \frac{1}{2} \prod_{i=1}^{N_r} \prod_{j=1}^{N_t} \exp\left(-\frac{\rho}{4} \delta_{min}'^2 |\bar{\mathbf{H}}_k(i,j)|^2\right), \qquad (20)$$

where $\delta_{min}' = \delta_{min} \sqrt{P_{tot}/N_{SS}}$. For the sake of mathematical tractability, let us assume that the channel between each of the transmit and receive antenna pairs has a fixed number of taps, i.e. $\|\mathbf{h}_{ij}\|_0 = L_a^{(ij)}$. This is a reasonable assumption, since the number of taps and their delays vary slowly compared to their amplitude and phase. Hence, we have $\bar{\mathbf{H}}_k(i,j) = \mathbf{h}_{ij}'(k) \sim \mathcal{CN}(0, \sigma_{ij}^2)$, where $\sigma_{ij}^2 = \sum_{k=0}^{L_a^{(ij)}-1} \sigma_{p_k^{(ij)}}^2$ so that $p_k^{(ij)}$ ($0 \leq k \leq L_a^{(ij)} - 1$) represent the baseband channel taps between the ith receive and the jth transmit antennas. Thus, we have

$$\text{PEP}(\mathbf{s} \to \mathbf{s}' | \bar{\mathbf{H}}_k) \leq \frac{1}{2} \prod_{i=1}^{N_r} \prod_{j=1}^{N_t} \exp\left(-\frac{\rho}{4} (\delta_{min}' \sigma_{ij})^2 |\hat{\mathbf{H}}_k(i,j)|^2\right), \qquad (21)$$

where $\hat{\mathbf{H}}_k(i,j) = \frac{\bar{\mathbf{H}}_k(i,j)}{\sigma_{ij}} \sim \mathcal{CN}(0,1)$. Since the channels between the various transmit and receive antenna pairs are

statistically independent, we have

$$\mathsf{PEP}(\mathbf{s} \to \mathbf{s}')$$

$$\leq \frac{1}{2} \prod_{i=1}^{N_r} \prod_{j=1}^{N_t} \mathbb{E}\left\{ \exp\left(-\frac{\rho}{4}(\delta'_{min}\sigma_{ij})^2 |\hat{\mathbf{H}}_k(i,j)|^2 \right) \right\}, \quad (22)$$

$$= \frac{1}{2} \prod_{i=1}^{N_r} \prod_{j=1}^{N_t} \frac{1}{1 + \frac{\rho}{4}(\delta'_{min}\sigma_{ij})^2}, \quad (23)$$

$$\approx \frac{1}{2} \left(\prod_{i=1}^{N_r} \prod_{j=1}^{N_t} \frac{4}{(\delta'_{min}\sigma_{ij})^2} \right) \frac{1}{\rho^{N_r N_t}}, \quad (24)$$

where (23) follows from the fact that $|\hat{\mathbf{H}}_k(i,j)|^2$ is an exponential random variable with unit mean and (24) corresponds to the high-SNR approximation, where $\rho \gg 1$. Thus, the upper bound on the probability of symbol error based on the union bound is given by

$$\mathsf{P}_e \leq \frac{1}{|\mathcal{S}|} \sum_{\mathbf{s} \in \mathcal{S}} \sum_{\mathbf{s} \neq \mathbf{s}' \in \mathcal{S}} \mathsf{PEP}(\mathbf{s} \to \mathbf{s}'), \quad (25)$$

$$\leq \frac{|\mathcal{S}| - 1}{2} \left(\prod_{i=1}^{N_r} \prod_{j=1}^{N_t} \frac{4}{(\delta'_{min}\sigma_{ij})^2} \right) \frac{1}{\rho^{N_r N_t}}. \quad (26)$$

From (26) it is evident that the proposed FDR-BF achieves full transmit as well as receive diversity gains. The above theoretical claims are validated through numerical simulations in Section IV.

2) Capacity Optimality: Assuming that the transmit symbols $\mathbf{s}_k$ are from the Gaussian alphabet, the mutual information [18] of the system in (8) with the proposed precoding is given by

$$MI_k = \log\left[\det(\mathbf{I}_{N_r} + \rho \bar{\mathbf{H}}_k \mathbf{P}_k \mathbf{P}_k^H \bar{\mathbf{H}}_k^H) \right]. \quad (27)$$

Substituting for $\mathbf{P}_k$ from (9) and $\mathbf{U}_k \mathbf{\Sigma}_k \mathbf{V}_k^H$ for $\bar{\mathbf{H}}_k$ in (27), we have

$$MI_k = \log\left[\det(\mathbf{I}_{N_{SS}} + \rho \mathbf{\Sigma}'_k \mathbf{\Theta}_{N_{SS}} \mathbf{\Theta}_{N_{SS}}^H \mathbf{\Sigma}'_k) \right]. \quad (28)$$

Since $\mathbf{\Theta}_{N_{SS}} \mathbf{\Theta}_{N_{SS}}^H = \mathbf{I}_{N_{SS}}$ due to the unitary property of FDR matrices [41], we have

$$MI_k = \log\left[\det(\mathbf{I}_{N_{SS}} + \rho \mathbf{\Sigma}_k'^2) \right], \quad (29)$$

$$= \sum_{i=1}^{N_{SS}} \log[1 + \rho P_k(i) \bar{\sigma}_k(i)^2], \quad (30)$$

which is essentially the capacity of the system in (8). Thus, the proposed scheme is deemed to be *information-lossless*, i.e. the maximum attainable mutual information of the proposed system is the same as the system's capacity.

3) Impact of Limited Feedback: In the above diversity analysis, we assumed that the transmitter has perfect CSI. In practice, this will not be the case owing to the limited number of bits available in the feedback channel. Explicitly, the transmitter would have a quantized channel $\bar{\mathbf{H}}_k^q$ instead of $\bar{\mathbf{H}}_k$ so that $\bar{\mathbf{H}}_k^q = \bar{\mathbf{H}}_k + \Delta\bar{\mathbf{H}}_k$, where $\Delta\bar{\mathbf{H}}_k$ is due to the quantization noise. Considering the proposed TDQ, let the quantized version of the time-domain channel $\mathbf{h}_{ij}$ be denoted by $\mathbf{h}_{ij}^q$. The instantaneous distortion due to the

quantization error is given by $\|\mathbf{h}_{ij} - \mathbf{h}_{ij}^q\|^2$. The corresponding frequency-domain distortion is given by $\|\mathbf{h}'_{ij} - \mathbf{h}_{ij}'^q\|^2 = \|\mathbf{F}_N(\mathbf{h}_{ij} - \mathbf{h}_{ij}^q)\|^2 = N\|\mathbf{h}_{ij} - \mathbf{h}_{ij}^q\|^2$. Thus, we have $\mathbb{E}[\|\mathbf{h}'_{ij} - \mathbf{h}_{ij}'^q\|^2] = N\mathbb{E}[\|\mathbf{h}_{ij} - \mathbf{h}_{ij}^q\|^2]$. When employing Algorithm 1 using the optimal number of quantization bits, we have $D_t = \mathbb{E}[\|\mathbf{h}_{ij} - \mathbf{h}_{ij}^q\|^2] \lesssim \sum_{i=0}^{L_q-1} \frac{\Delta_i^2}{12} = \sum_{i=0}^{L_q-1} \frac{B_i \sigma_i^2}{3 \log e} 2^{-2\bar{B}_i}$ [37]. Thus, the average distortion associated with each of the taps reduces exponentially with the number of quantization bits $\bar{B}_i$, which is also evident from Fig. 2. Since $\|\Delta\bar{\mathbf{H}}_k\|^2 \propto \sum_{i=1}^{N_r} \sum_{j=1}^{N_t} \|\mathbf{h}'_{ij} - \mathbf{h}_{ij}'^q\|^2$, we can expect $\|\Delta\bar{\mathbf{H}}_k\|^2$ to be negligible, when the number of bits employed for quantizing each of the links between the transmit and receive antenna pair is sufficiently high. In the next section, we show that about 30 quantization bits, which corresponds to a distortion level of $D_t = 10^{-2}$ (refer Fig. 2), would be sufficient to attain the same performance as that attained by having perfect CSI.

IV. SIMULATION RESULTS AND DISCUSSIONS

Simulation Scenario

In all our simulations, we assume $N_{CP} = 32$ and $N = 64$ subcarriers. The BER performance of all the schemes is evaluated by assuming perfect CSI and an ML detector at the receiver. For evaluating a BER of 10^{-t}, we have employed at least 10^{t+1} bits in all our simulations. All the MIMO schemes assume $N_t = N_r = N_{SS} = 2$. The MIMO scheme employing SVD based BF [18] is referred to as MIMO-SVD. The MIMO scheme employing strongest Eigenmode transmission is referred to as EMT. The single-input multiple-output (SIMO) system corresponds to a system having $N_t = 1$ and $N_r = 2$. Each transmitted OFDM symbol is appropriately normalized to ensure that the average signal energy is the same across all the schemes considered in the paper. For the ease of presentation, we use the following definition of datarate:

$$\text{rate} = \frac{N_{SS} \times \text{No. of information bits per OFDM stream}}{N},$$

which ignores the overhead due to CP. Owing to the limited space, we consider only the two extreme elevation angles in our simulation studies, i.e. $\Psi \in \{30°, 7.5°\}$. The performance curves associated with the other two elevation angles are observed to fall between the curves associated with the above two angles and are not included. For simulating a coded system, we consider a convolutional encoder associated with the industry-standard octal generator polynomials, $g_0 = 133_8$ and $g_1 = 171_8$ of coding rate 1/2 as specified in 18.3.5.6 of the 802.11n/ac standard [32]. The encoded bits are interleaved using a block-interleaver of appropriate length, which depends on the operating datarate. At the receiver, the ML decoded bits are deinterleaved and passed on to the Viterbi decoder for obtaining the information bits.

A. Comparison With the Existing Schemes

Assuming perfect CSIT, let us now compare the BER performance of the proposed FDR-BF to that of the classic SIMO, MIMO-VBLAST, MIMO-SVD and GMD [20] schemes. Fig. 3 portrays the BER performance of the aforementioned schemes operating at a datarate of 4 bpcu and
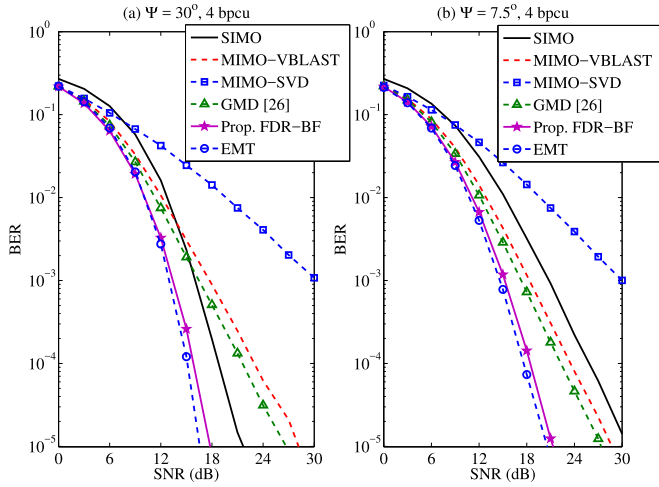
Fig. 3. Comparison of the BER performance of the proposed FDR-BF scheme with that of SIMO, MIMO, MIMO-SVD, EMT and GMD [20] schemes. All the systems are assumed to be operating at a rate of 4 bpcu. Plot (a) corresponds to the elevation angle of $\Psi = 30°$, whereas Plot (b) corresponds to that of $\Psi = 7.5°$.
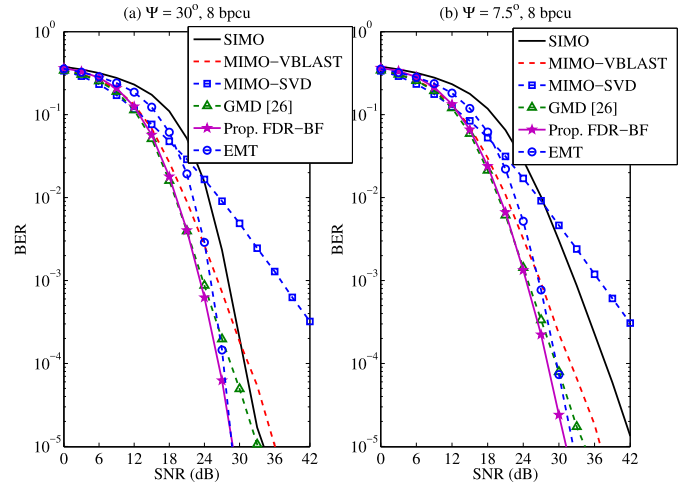

Fig. 4. Comparison of the BER performance of the proposed FDR-BF scheme with that of SIMO, MIMO, MIMO-SVD, EMT and GMD [20] schemes. All the systems are assumed to be operating at a rate of 8 bpcu. Plot (a) corresponds to the elevation angle of $\Psi = 30°$, whereas Plot (b) corresponds to that of $\Psi = 7.5°$.

elevation angles of $\Psi \in \{30°, 7.5°\}$. Specifically, Fig. 3(a) corresponds to the elevation angle of $\Psi = 30°$, whereas Fig. 3(b) corresponds to that of $\Psi = 7.5°$. The following observations can be made from Fig. 3:

1) The MIMO-SVD scheme performs poorly compared to the other schemes owing to the unequal SNR over the parallel subchannels. The effective BER performance at high SNR is dictated by the subchannel associated with the lowest singular value.

2) The SIMO system performs better than the MIMO-VBLAST and GMD schemes at $\Psi = 30°$ and worse when $\Psi = 7.5°$. This is due to the relatively shorter delay spread at $\Psi = 30°$, which enables the ML detector to attain higher power gain across all the subcarriers. When the delay spread is longer as in the case of $\Psi = 7.5°$, the chances of some subcarriers being in deep fade would be high.

3) The GMD scheme performs better than the MIMO-VBLAST as well as the MIMO-SVD schemes, owing to the beamforming gain as well as due to having equal SNRs across all the parallel subchannels.

4) The proposed FDR-BF scheme outperforms the other schemes at both the elevation angles. Specifically, at a BER of 10^{-5} the proposed scheme provides an SNR gain of about 3dB compared to the SIMO system at $\Psi = 30°$ and about 6dB compared to the GMD scheme at $\Psi = 7.5°$.

5) The performance of the FDR-BF scheme is comparable to that of EMT when operating at 4 bpcu, while the proposed scheme outperforms the EMT at 8 bpcu as evident from Fig. 4.

Figure 4 provides the BER performance of the aforementioned schemes operating at a datarate of 8 bpcu. Similar observations to 1)-4) hold for this case as well. It can be observed from Fig. 3 and Fig. 4 that both the proposed as well as the existing schemes suffer from performance loss, when the elevation angle drops. Fig. 5 provides the BER performance of
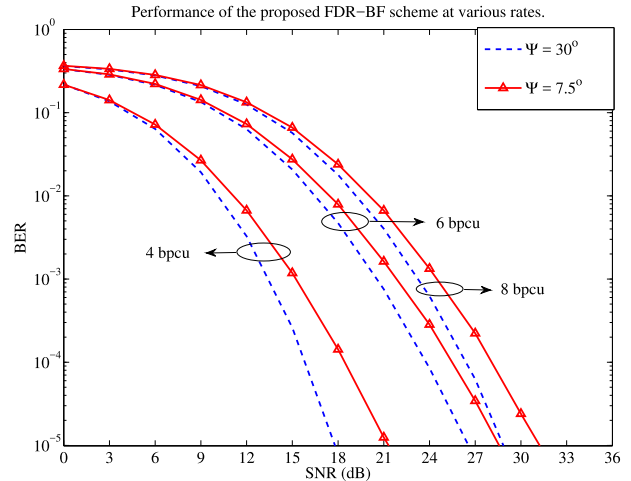

Fig. 5. BER performance of the proposed FDR-BF scheme at various rates and elevation angles.

the proposed scheme operating at various rates and elevation angles. It is evident from Fig. 5 that lower elevations result in performance degradation compared to higher elevation angles at all datarates. Specifically, there is a performance degradation of 3dB at a datarate of 4bpcu and about 2dB in case of 6 and 8bpcu.

Remark 1: In case of multi-user beamforming, where multiple users are located at different elevation angles with respect to the aerial transmitter, the elevation angle should be taken into account in addition to the SNR of each user in order to decide the modulation and coding scheme for each user.

B. Proposed TDQ vs. FDQ of 802.11 [32]

Let us compare the BER performance of the proposed scheme operating both with perfect and with quantized CSI. The quantized CSI is obtained by employing the proposed TDQ that employs the optimal number of quantization bits given in (2). For the three distortion levels
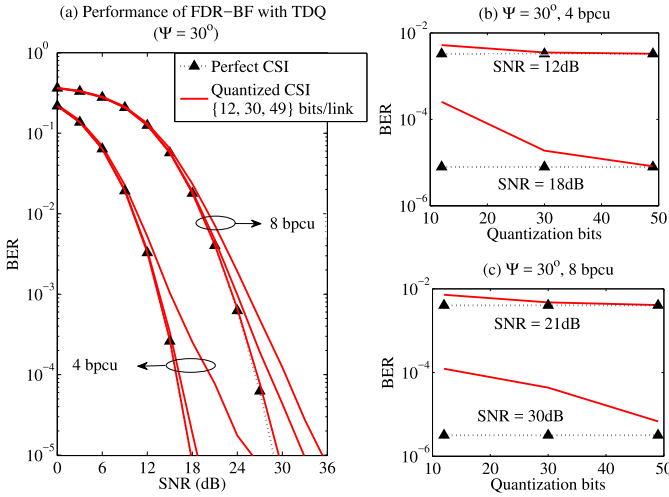
Fig. 6.   Comparison of the BER performance of the proposed FDR-BF scheme operating at 4 and 8 bpcu with the aid of perfect and quantized CSI at the transmitter. The aerial transmitter is assumed to be at an elevation of $\Psi = 30°$. Plot (a) depicts the variation in BER as a function of SNR, whereas Plot (b) and Plot (c) depict the variation in BER as a function of the number of quantization bits employed in TDQ.
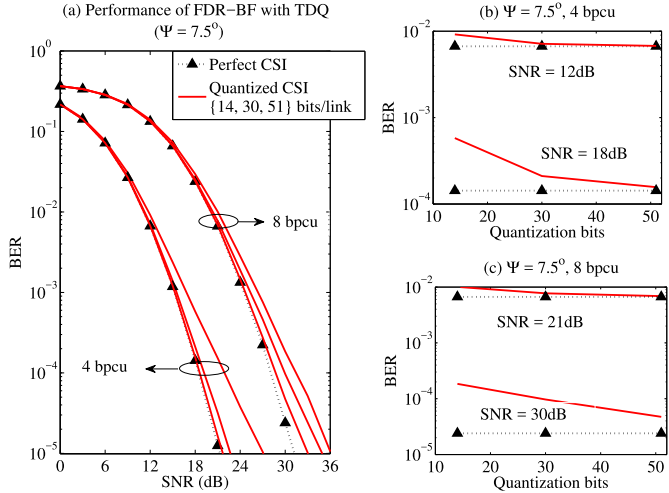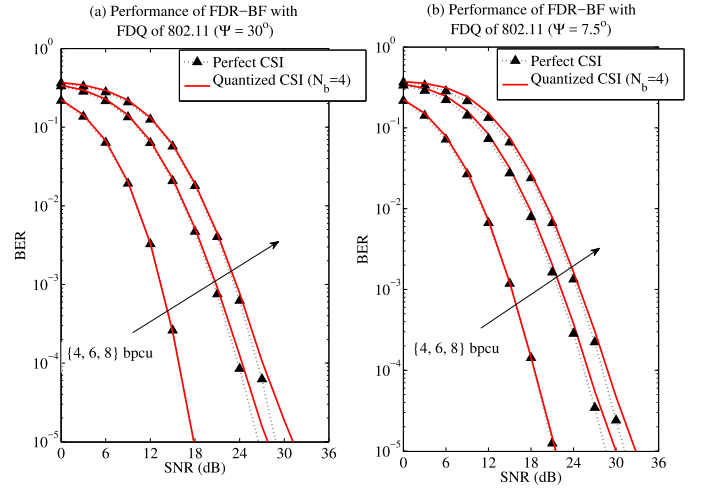

Fig. 8.   Comparison of the BER performance of the proposed FDR-BF scheme operating at various rates with the aid of perfect CSI and quantized CSI obtained based on FDQ of 802.11 [32]. The FDQ is assumed to employ $N_b = 4$ bits, which corresponds to $N_{FDQ} = 1820$ bits. Plot (a) corresponds to the elevation angle of $\Psi = 30°$, whereas Plot (b) corresponds to that of $\Psi = 7.5°$.

Let us compare the BER performance of the proposed scheme operating with quantized CSI obtained based on the FDQ of 802.11. We assume an FDQ employing $N_b = 4$ bits [32], which corresponds to the lowest number of quantization bits supported by the standard. Note that $N_b = 4$ corresponds to $N_{FDQ} = 1820$ bits. Figure 8 provides the BER performance of the proposed FDR-BF scheme operating at various rates both with perfect and with FDQ based CSI for $\Psi = 30°$ and $\Psi = 7.5°$. It is evident from both Fig. 8(a) and Fig. 8(b) that the BER performance of the proposed scheme operating with quantized CSI is essentially the same as that of perfect CSI. Thus, the minimum number of quantization bits supported by the standard would be sufficient to attain the optimal performance and hence the higher quantization resolutions that correspond to $N_b \in \{5, 6, 8\}$ [32] may not be required in the aerial communication scenario. This is mainly due to the sparsity of the A2G multipath channel, which renders the frequency-domain channel somewhat flat compared to that of the more rich indoor scattering environment.

Remark 2: The proposed scheme operating with the aid of TDQ attains nearly the same optimal performance as that attained by employing FDQ of 802.11. Considering the fact that the number of quantization bits required in case of TDQ is far lesser than that of FDQ, it would be beneficial to relook at the medium access control (MAC)-level beamforming training protocol of the existing 802.11 standard, which may help in significantly reducing the overhead involved in conveying the quantized CSI.

Fig. 7.   Comparison of the BER performance of the proposed FDR-BF scheme operating at 4 and 8 bpcu with the aid of perfect and quantized CSI at the transmitter. The aerial transmitter is assumed to be at an elevation of $\Psi = 7.5°$. Plot (a) depicts the variation in BER as a function of SNR, whereas Plot (b) and Plot (c) depict the variation in BER as a function of the number of quantization bits employed in TDQ.

$\{10^{-1}, 10^{-2}, 10^{-3}\}$, the optimal number of quantization bits are $\{12, 30, 49\}$ for $\Psi = 30°$ and $\{14, 30, 51\}$ for $\Psi = 7.5°$. Figure 6 compares the BER performance of the proposed FDR-BF scheme operating both with perfect and with quantized CSI at $\Psi = 30°$. It is evident from Fig. 6(a) that the proposed scheme operating with a CSI quantized to 30 bits attains essentially the same performance as that of the perfect CSI at low to moderate SNRs. Fig. 6(b) and Fig.6(c) depict the variation in the BER as a function of the number of quantization bits employed in TDQ for the two datarates of 4 and 8 bpcu, respectively.

Figure 7 provides the BER performance of the proposed scheme operating both with perfect and with quantized CSI for $\Psi = 7.5°$. Similar observations to those of Fig. 6 hold for this case as well.

C. Coded BER Performance

The coded BER performance of the proposed as well as that of the MIMO system are provided for the datarates of 2 and 3 bpcu in Fig. 9, where both the transmitter as well as the receiver are assumed to have perfect CSI. The performance of the uncoded MIMO system is also provided in order to show the potentially attainable BER performance by varying
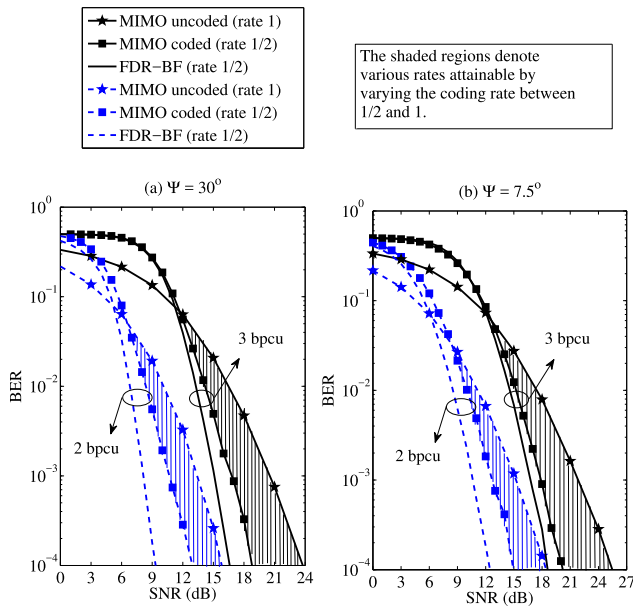
Fig. 9. Comparison of the coded BER performance of the proposed FDR-BF scheme with that of the MIMO scheme. The BER performance of the uncoded MIMO system is also provided for comparison. Plot (a) corresponds to the elevation angle of $\Psi = 30°$, whereas Plot (b) corresponds to that of $\Psi = 7.5°$.

the coding rate. This corresponds to the shaded regions in both Fig. 9(a) and Fig. 9(b). It can be seen from Fig. 9(a) and Fig. 9(b) that when operating at 2 bpcu, the proposed scheme provides an SNR gain of about 4dB with respect to the coded MIMO system at $\Psi = 30°$ and about 2.5dB at $\Psi = 7.5°$. These SNR gains enable us to extend the signal range and hence the coverage area. When operating at 3 bpcu, the SNR gain attained by the proposed scheme with respect to the MIMO system is about 2.5dB at $\Psi = 30°$ and about 2dB at $\Psi = 7.5°$.

Figure 10 compares the coded BER performance of the proposed scheme operating at various rates and employing: (a) perfect CSI, (b) CSI obtained based on TDQ with 30 bits/link and (c) CSI obtained based on FDQ of 802.11 with $N_b = 4$. Figure 10(a) corresponds to an elevation angle of $\Psi = 30°$, while Figure 10(b) corresponds to an elevation of $\Psi = 7.5°$. It is evident from Figure 10(a) and Figure 10(b) that the proposed scheme operating with quantized CSI obtained from TDQ or FDQ of 802.11 attains the same performance as that of the perfect CSI. Thus, the proposed TDQ which requires only a few feedback bits is an attractive solution compared to the existing FDQ of 802.11 standard.

V. CONCLUSIONS AND FUTURE DIRECTIONS

We have provided a statistical model for the A2G multipath channel, which is beneficial for the design and analysis of aerial communication systems deployed as LAPs. The proposed A2G channel model was utilized for designing a time-domain quantizer, which was shown to require much less quantization bits than the frequency-domain quantizer employed in the 802.11n/ac standard. Furthermore, a beamforming aided full-diversity scheme was proposed with the aid of full-diversity rotation matrices. The symbol error probability of the proposed scheme was evaluated analytically and the
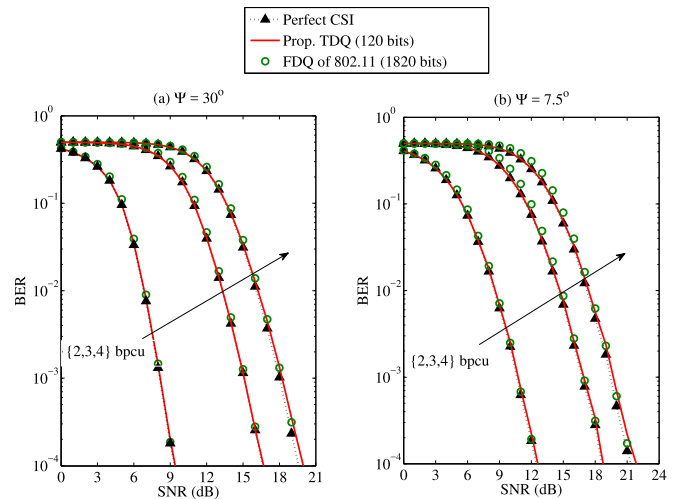

Fig. 10. Comparison of the coded BER performance of the proposed FDR-BF scheme operating with the aid of perfect CSI and that obtained based on the proposed TDQ as well as the FDQ of 802.11 [32]. The three rates of 2, 3 and 4 bpcu are attained by employing 4-QAM, 8-QAM, and 16-QAM in conjunction with a rate-1/2 convolutional code, respectively. Plot (a) corresponds to the elevation angle of $\Psi = 30°$, whereas Plot (b) corresponds to that of $\Psi = 7.5°$.

attainable diversity order was shown to be $N_t N_r$. Furthermore, the proposed scheme was shown to be *information-lossless*. It was shown through numerical simulations that the proposed scheme outperforms several existing schemes when operating at various elevation angles. Furthermore, the BER performance of the proposed scheme was studied under quantized CSI obtained based on the proposed TDQ as well as the FDQ of 802.11. It was observed in both coded as well as uncoded scenarios that the BER performance attained by the proposed scheme employing the TDQ is the same as that of perfect CSI, despite using far less quantization bits than that required by the FDQ of 802.11n/ac.

In all our studies, we have fixed the length of CP to be $N_{CP} = 32$, which caters for the maximum multipath delay of $1.6\mu s$. This can be reduced, especially at higher elevations, where the RMS delay spread is small. Note that the 802.11n/ac supports two guard intervals: $0.4\mu s$ and $0.8\mu s$. These would be too large for higher elevations, where the RMS delay spread is only of the order of 10's of nanoseconds. It would be beneficial to study the impact of having lower CP lengths on the performance at various elevation angles. The 802.11n/ac employs cyclic shift delays (CSD) [45] across multiple streams in order to exploit multipath delay diversity as well as to avoid undesirable beamforming effects when transmitting the same signal across all the transmit antennas. This would be only beneficial in rich multipath scattering. In case of sparse multipath scattering as in the case of A2G channel, it would be highly inefficient [46]. Thus, it is important to study the impact of CSD on the performance at various elevation angles.

REFERENCES

[1] S. Chandrasekharan *et al.*, "Designing and implementing future aerial communication networks," *IEEE Commun. Mag.*, vol. 54, no. 5, pp. 26–34, May 2016.

[2] Y. Zeng, R. Zhang, and T. J. Lim, "Wireless communications with unmanned aerial vehicles: Opportunities and challenges," *IEEE Commun. Mag.*, vol. 54, no. 5, pp. 36–42, May 2016.

[3] S. Hayat, E. Yanmaz, and R. Muzaffar, "Survey on unmanned aerial vehicle networks for civil applications: A communications viewpoint," *IEEE Commun. Surveys Tuts.*, vol. 18, no. 4, pp. 2624–2661, 4th Quart., 2016.

[4] J.-J. Wang, C.-X. Jiang, Z. Han, Y. Ren, R. G. Maunder, and L. Hanzo, "Taking drones to the next level: Cooperative distributed unmanned-aerial-vehicular networks for small and mini drones," *IEEE Veh. Technol. Mag.*, vol. 12, no. 3, pp. 73–82, Sep. 2017.

[5] A. Al-Hourani, S. Kandeepan, and S. Lardner, "Optimal LAP altitude for maximum coverage," *IEEE Wireless Commun. Lett.*, vol. 3, no. 6, pp. 569–572, Dec. 2014.

[6] A. Vilhar, A. Hrovat, T. Javornik, and M. Mohorcic, "Experimental analysis of wireless temporary networks deployed by low altitude platforms," in *Proc. IEEE 18th Int. Workshop Comput. Aided Modeling Design Commun. Links Netw. (CAMAD)*, Berlin, Germany, Sep. 2013, pp. 238–242.

[7] I. Bucaille, S. Hethuin, A. Munari, R. Hermenier, T. Rasheed, and S. Allsopp, "Rapidly deployable network for tactical applications: Aerial base station with opportunistic links for unattended and temporary events ABSOLUTE example," in *Proc. IEEE Mil. Commun. Conf. (MILCOM)*, San Diego, CA, USA, Nov. 2013, pp. 1116–1120.

[8] J.-K. Zhang, S. Chen, R. G. Maunder, R. Zhang, and L. Hanzo, "Adaptive coding and modulation for large-scale antenna array-based aeronautical communications in the presence of co-channel interference," *IEEE Trans. Wireless Commun.*, vol. 17, no. 2, pp. 1343–1357, Feb. 2018.

[9] Z. Wu, H. Kumar, and A. Davari, "Performance evaluation of OFDM transmission in UAV wireless communication," in *Proc. 27th Southeastern Symp. Syst. Theory (SSST)*, Mar. 2005, pp. 6–10.

[10] E. Yanmaz, R. Kuschnig, and C. Bettstetter, "Achieving air-ground communications in 802.11 networks with three-dimensional aerial mobility," in *Proc. IEEE INFOCOM*, Turin, Italy, Apr. 2013, pp. 120–124.

[11] M. Asadpour, D. Giustiniano, and K. A. Hummel, "From ground to aerial communication: Dissecting WLAN 802.11n for the drones," in *Proc. ACM Int. Workshop Wireless Netw. Testbeds Exp. Eval. Characterization (WiNTECH)*, Miami, FL, USA, 2013, pp. 25–32.

[12] E. Yanmaz, S. Hayat, J. Scherer, and C. Bettstetter, "Experimental performance analysis of two-hop aerial 802.11 networks," in *Proc. IEEE Wireless Commun. Netw. Conf. (WCNC)*, Istanbul, Turkey, Apr. 2014, pp. 3118–3123.

[13] S. Hayat, E. Yanmaz, and C. Bettstetter, "Experimental analysis of multipoint-to-point UAV communications with IEEE 802.11n and 802.11ac," in *Proc. IEEE 26th Annu. Int. Symp. Pers., Indoor, Mobile Radio Commun. (PIMRC)*, Hong Kong, Aug./Sep. 2015, pp. 1991–1996.

[14] A. Guillen-Perez, R. Sanchez-Iborra, M. D. Cano, J. C. Sanchez-Aarnoutse, and J. Garcia-Haro, "WiFi networks on drones," in *Proc. ITU Kaleidoscope, ICTs Sustain. World (ITU WT)*, Bangkok, Thailand, 2016, pp. 1–8.

[15] H. Jamal and D. W. Matolak, "Multicarrier air to ground MIMO communication system performance," in *Proc. IEEE 84th Veh. Technol. Conf. (VTC-Fall)*, Montreal, QC, Canada, Sep. 2016, pp. 1–5.

[16] C. Zhang and Y. Hui, "Broadband air-to-ground communications with adaptive MIMO datalinks," in *Proc. IEEE/AIAA 30th Digit. Avionics Syst. Conf.*, Seattle, WA, USA, Oct. 2011, pp. 4D4-1–4D4-10.

[17] J. Chen *et al.*, "Long-range and broadband aerial communication using directional antennas (ACDA): Design and implementation," *IEEE Trans. Veh. Technol.*, vol. 66, no. 12, pp. 10793–10805, Dec. 2017.

[18] D. Tse and P. Viswanath, *Fundamentals of Wireless Communications*. Cambridge, U.K.: Cambridge Univ. Press, 2005.

[19] Y. Jiang, W. Hager, and J. Li, "The geometric mean decomposition," *Linear Algebra Appl.*, vol. 396, pp. 373–384, Feb. 2005.

[20] Y. Jiang, J. Li, and W. W. Hager, "Joint transceiver design for MIMO communications using geometric mean decomposition," *IEEE Trans. Signal Process.*, vol. 53, no. 10, pp. 3791–3803, Oct. 2005.

[21] Y. Jiang, J. Li, and W. M. Hager, "Uniform channel decomposition for MIMO communications," *IEEE Trans. Signals Process.*, vol. 53, no. 11, pp. 4283–4294, Nov. 2005.

[22] S. Zhou and G. B. Giannakis, "Optimal transmitter eigen-beamforming and space-time block coding based on channel mean feedback," *IEEE Trans. Signal Process.*, vol. 50, no. 10, pp. 2599–2613, Oct. 2002.

[23] Z. Lei, F. P. S. Chin, and Y.-C. Liang, "Combined beamforming with space-time block coding for wireless downlink transmission," in *Proc. IEEE 56th Veh. Technol. Conf.*, vol. 4, Sep. 2002, pp. 2145–2148.

[24] S. Ekbatani and H. Jafarkhani, "Combining beamforming and space-time coding using quantized feedback," *IEEE Trans. Wireless Commun.*, vol. 7, no. 3, pp. 898–908, Mar. 2008.

[25] S. Ekbatani and H. Jafarkhani, "Combining beamforming and space-time coding using noisy quantized feedback," *IEEE Trans. Commun.*, vol. 57, no. 5, pp. 1280–1286, May 2009.

[26] H. Wang, Y. Li, X. G. Xia, and S. Liu, "Unitary and non-unitary precoders for a limited feedback precoded OSTBC system," *IEEE Trans. Veh. Technol.*, vol. 62, no. 4, pp. 1646–1654, May 2013.

[27] W. G. Newhall *et al.*, "Wideband air-to-ground radio channel measurements using an antenna array at 2 GHz for low-altitude operations," in *Proc. IEEE Mil. Commun. Conf. (MILCOM)*, vol. 2, Oct. 2003, pp. 1422–1427.

[28] T. J. Willink, C. C. Squires, G. W. K. Colman, and M. T. Muccio, "Measurement and characterization of low-altitude air-to-ground MIMO channels," *IEEE Trans. Veh. Technol.*, vol. 65, no. 4, pp. 2637–2648, Apr. 2016.

[29] D. W. Matolak and R. Sun, "Air–ground channel characterization for unmanned aircraft systems—Part III: The suburban and near-urban environments," *IEEE Trans. Veh. Technol.*, vol. 66, no. 8, pp. 6607–6618, Aug. 2017.

[30] X. Cai *et al.*, "Low altitude UAV propagation channel modelling," in *Proc. 11th Eur. Conf. Antennas Propag. (EUCAP)*, Paris, France, Mar. 2017, pp. 1443–1447.

[31] J. B. Andersen, T. S. Rappaport, and S. Yoshida, "Propagation measurements and models for wireless communications channels," *IEEE Commun. Mag.*, vol. 33, no. 1, pp. 42–49, Jan. 1995.

[32] *Part 11: Wireless LAN Medium Access Control (MAC) and Physical Layer (PHY) Specifications*, IEEE Standard 802.11, Mar. 2012.

[33] K. K. Mukkavilli, A. Sabharwal, E. Erkip, and B. Aazhang, "On beamforming with finite rate feedback in multiple-antenna systems," *IEEE Trans. Inf. Theory*, vol. 49, no. 10, pp. 2562–2579, Oct. 2003.

[34] V. Raghavan, R. W. Heath, Jr., and A. M. Sayeed, "Systematic codebook designs for quantized beamforming in correlated MIMO channels," *IEEE J. Sel. Areas Commun.*, vol. 25, no. 7, pp. 1298–1310, Sep. 2007.

[35] H. Shirani-Mehr and G. Caire, "Channel state feedback schemes for multiuser MIMO-OFDM downlink," *IEEE Trans. Commun.*, vol. 57, no. 9, pp. 2713–2723, Sep. 2009.

[36] Y.-S. Jeon, H.-M. Kim, Y.-S. Cho, and G.-H. Im, "Time-domain differential feedback for massive MISO-OFDM systems in correlated channels," *IEEE Trans. Commun.*, vol. 64, no. 2, pp. 630–642, Feb. 2016.

[37] R. M. Gray and D. L. Neuhoff, "Quantization," *IEEE Trans. Inf. Theory*, vol. 44, no. 6, pp. 2325–2383, Oct. 1998.

[38] T. M. Cover and J. A. Thomas, *Elements of Information Theory*. New York, NY, USA: Wiley, 1991.

[39] M. O. Damen, K. Abed-Meraim, and J. C. Belfiore, "Diagonal algebraic space-time block codes," *IEEE Trans. Inf. Theory*, vol. 48, no. 3, pp. 628–636, Mar. 2002.

[40] E. Bayer-Fluckiger, F. Oggier, and E. Viterbo, "New algebraic constructions of rotated Zn-lattice constellations for the Rayleigh fading channel," *IEEE Trans. Inf. Theory*, vol. 50, no. 4, pp. 702–714, Apr. 2004.

[41] E. Viterbo. *Full Diversity Rotations*. Accessed: Mar. 16, 2005. [Online]. Available: http://www.ecse.monash.edu.au/staff/eviterbo/rotations/rotations.html

[42] S. Bergman and B. Bjorn, "Lattice-based linear precoding for MIMO channels with transmitter CSI," *IEEE Trans. Signal Process.*, vol. 56, no. 7, pp. 2902–2914, Jul. 2008.

[43] A. Sakzad and V. Emanuele, "Full diversity unitary precoded integer-forcing," *IEEE Trans. Wireless Commun.*, vol. 14, no. 8, pp. 4316–4327, Aug. 2015.

[44] S.-H. Chang, P. C. Cosman, and L. B. Milstein, "Chernoff-type bounds for the Gaussian error function," *IEEE Trans. Commun.*, vol. 59, no. 11, pp. 2939–2944, Nov. 2011.

[45] A. Dammann and S. Kaiser, "Transmit/receive-antenna diversity techniques for OFDM systems," *Eur. Trans. Telecommun.*, vol. 13, no. 5, pp. 531–538, 2002.

[46] A. Dammann, R. Raulefs, and S. Plass, "Soft cyclic delay diversity and its performance for DVB-T in rician channels," in *Proc. IEEE IEEE Global Telecommun. Conf. (GLOBECOM)*, Washington, DC, USA, 2007, pp. 4210–4214.

Rakshith Rajashekar (M'14–SM'17) received the B.E. degree in electrical communication engineering from Visvesvaraya Technological University, Belgaum, India, in 2007, and the Ph.D. degree from the Department of Electrical Communication Engineering, Indian Institute of Science, India, in 2014. He was with Accord Software & Systems, Bengaluru, India, as a Systems Engineer, from 2007 to 2009, and as a Senior Scientist at Broadcom Communications, Bengaluru, from 2014 to 2015. He is currently a Research Fellow with the University of Southampton, U.K. His research interests include antenna selection in MIMO systems, differential communication, millimeter-wave communication, communication between drones with a focus on space–time signal processing and coding. He was a recipient of the Special Recognition Award from Broadcom Communications, India, and the Dean's Award from the University of Southampton, for excellence in research. He received the Best Reviewer Award from the IEEE TRANSACTIONS ON WIRELESS COMMUNICATIONS, the IEEE TRANSACTIONS ON COMMUNICATIONS, and the IEEE WIRELESS COMMUNICATIONS LETTERS.

Marco Di Renzo (S'05–AM'07–M'09–SM'14) was born in L'Aquila, Italy, in 1978. He received the Laurea *(cum laude)* and Ph.D. degrees in electrical engineering from the University of L'Aquila, L'Aquila, in 2003 and 2007, respectively, and the D.Sc. degree (HDR) from University Paris-Sud, Paris, France, in 2013. Since 2010, he has been a CNRS Associate Professor (Chargé de Recherche Titulaire CNRS) with the Laboratory of Signals and Systems, Paris-Saclay University–CNRS, CentraleSupélec, University of Paris-Sud. He is currently an Adjunct Professor with the University of Technology Sydney, Australia, a Visiting Professor with the University of L'Aquila, and a Co-Founder of the university spinoff company WEST Aquila s.r.l., Italy. He is a Distinguished Lecturer of the IEEE Vehicular Technology Society and the IEEE Communications Society. He is the Project Coordinator of the European-funded projects H2020-MSCA ETN-5Gwireless and H2020-MSCA ETN-5Gaura. He was a recipient of several awards, including the 2013 IEEE-COMSOC Best Young Researcher Award for Europe, Middle East, and Africa (EMEA Region), the 2013 NoE-NEWCOM Best Paper Award, the 2014–2015 Royal Academy of Engineering Distinguished Visiting Fellowship, the 2015 IEEE Jack Neubauer Memorial Best System Paper Award, the 2015–2018 CNRS Award for Excellence in Research and in Advising Doctoral Students, the 2016 MSCA Global Fellowship (declined), the 2017 SEE-IEEE Alain Glavieux Award, the 2018 IEEE ICNC Silver Contribution Award, and six best paper awards at IEEE conferences (2012 and 2014 IEEE CAMAD, 2013 IEEE VTC-Fall, 2014 IEEE ATC, 2015 IEEE ComManTel, and 2017 IEEE SigTelCom). He serves as the Associate Editor-in-Chief for the IEEE COMMUNICATIONS LETTERS, and as an Editor for the IEEE TRANSACTIONS ON COMMUNICATIONS and the IEEE TRANSACTIONS ON WIRELESS COMMUNICATIONS.

K. V. S. Hari (M'92–SM'97–F'15) received the B.E. degree from Osmania University, Hyderabad, India, in 1983, the M.Tech. degree from the IIT Delhi, New Delhi, India, in 1985, and the Ph.D. degree from the University of California at San Diego, La Jolla, CA, USA, in 1990. Since 1992, he has been with the Department of Electrical Communication Engineering, Indian Institute of Science, Bengaluru, India, where he is currently a Professor and a Coordinator of the Statistical Signal Processing Laboratory. He was an Affiliated Professor with the Department of Signal Processing, KTH Royal Institute of Technology, Stockholm, Sweden, from 2010 to 2016. He has been a Visiting Faculty Member with Stanford University, Stanford, CA, USA, the KTH Royal Institute of Technology, and Aalto University, Espoo, Finland (formerly the Helsinki University of Technology). While at Stanford University, he worked on multiple-input multiple-output (MIMO) wireless channel modeling and has co-authored the Worldwide Interoperability for Microwave Access standard on wireless channel models for fixed-broadband wireless communication systems, which proposed the Stanford University Interim channel models. He was also with the Defence Electronics Research Laboratory, Hyderabad, and the Research and Training Unit for Navigational Electronics, Osmania University. He is also an academic entrepreneur and a Co-Founder of the company ESQUBE Communication Solutions, Bangaluru. His research interests include the development of signal processing algorithms for MIMO wireless communication systems, sparse signal recovery problems, indoor positioning, assistive technologies for the elderly, and neuroscience. He received the Institution of Electronics and Telecommunication Engineers S. V. C. Aiya Award for Excellence in Telecom Education and the Distinguished Alumnus Award from the Osmania University College of Engineering. He is a fellow of the Indian NAE. He was an Editor of *EURASIP Journal Signal Processing* (Elsevier) (2006–2016) and a Senior Associate Editor of Indian Academy of Sciences journal *Sādhanā* (Springer).

Lajos Hanzo (M'91–SM'92–F'04) received the D.Sc. degree in electronics in 1976 and the Ph.D. degree in 1983. During his 40-year career in telecommunications, he has held various research and academic posts in Hungary, Germany, and the U.K. Since 1986, he has been with the School of Electronics and Computer Science, University of Southampton, U.K., where he holds the Chair in telecommunications. He was a Chaired Professor with Tsinghua University, Beijing. In 2016, he was admitted to the Hungarian Academy of Science. He is currently directing an academic research team, working on a range of research projects in the field of wireless multimedia communications sponsored by industry, the Engineering and Physical Sciences Research Council, U.K., the European Research Council's Advanced Fellow Grant, and the Royal Society's Wolfson Research Merit Award. He has successfully supervised 111 Ph.D. students, co-authored 18 John Wiley/IEEE Press books on mobile radio communications totaling in excess of 10 000 pages, published 1685 research contributions at *IEEE Xplore*, acted both as a TPC and general chair of IEEE conferences, presented keynote lectures, and has been awarded a number of distinctions. He is a fellow of the Royal Academy of Engineering, IET, and EURASIP. In 2009, he was a recipient of the honorary doctorate by the Technical University of Budapest and in 2015 by The University of Edinburgh. He is an enthusiastic supporter of industrial and academic liaison, and he offers a range of industrial courses. He is also the Governor of the IEEE VTS. From 2008 to 2012, he was the Editor-in-Chief of the IEEE Press. For further information on research in progress and associated publications, please refer to http://www-mobile.ecs.soton.ac.uk. He has over 38 000 citations and an H-index of 78.